^{13}C-NMR of the Deoxyribose Sugars in Four DNA Oligonucleotide Duplexes: Assignment and Structural Features†

Steven R. LaPlante,‡,§ Nilo Zanatta,‖ Anna Hakkinen,⊥ Andrew H.-J. Wang,▽ and Philip N. Borer*,‡

Center for Science and Technology, Chemistry Department, Syracuse University, Syracuse, New York 13244-4100

Received November 24, 1993⊛

ABSTRACT: Natural-abundance ^{13}C-NMR spectra have been obtained for four self-complementary DNA oligonucleotides: $[d(TAGCGCTA)]_2$, $[d(GGTATACC)]_2$, $[d(CG)_3]_2$, and $[d(TCGCG)]_2$; this paper focuses on the deoxyribose resonances. Assignments were made by a combination of the two-dimensional proton-detected heteronuclear correlation experiment and comparison of 1D spectra, accounting for ^{31}P coupling, base composition, and similarities in chemical shift versus temperature profiles (δ *vs* T). Large shielding and deshielding of the sugar resonances (between 2.0 and −1.9 ppm) are observed upon thermal dissociation of the duplex. The shapes of the δ *vs* T profiles correlate strongly with the purine/pyrimidine nature of the base attached at C1′ in these duplexes that have a substantial fraction of residues within alternating purine–pyrimidine sequences. The correlation is primarily associated with changes in the equilibrium distribution of furanose pseudorotational states that may arise in part from the relief of interstrand purine–purine steric clashes.

Reports on the ^{13}C-NMR[1] of DNA oligonucleotides show resolution of individual resonances, where (i) the chemical shifts of the bases are most sensitive to hydrogen bonding (Borer et al., 1984, 1988; LaPlante et al., 1988a; Zanatta et al., 1987; Petersen & Led, 1981; Iwahashi & Kyogoku, 1976; Newmark & Cantor, 1968) and steric effects (Stone et al., 1986; LaPlante et al., 1988a) and (ii) the carbon signals of the sugar moieties are profoundly affected by changes in the equilibrium blend of pseudorotational states [called ψ-states in this paper—see Saenger (1984) for definition and nomenclature of the ψ-states and their relation to the endocyclic torsion angles; Lankhorst et al., 1983; Borer et al., 1984; Stone et al., 1986; Varani & Tinoco, 1991)]. ^{13}C-NMR is also a useful probe of the overall and internal dynamics in DNA (Levy et al., 1981; 1983; Borer et al., 1984, 1992; Zanatta et al., 1987; Williamson & Boxer, 1989; Eimer et al., 1990). Another paper (Borer et al., 1984) describes a model-free analysis of the ^{13}C-NMR relaxation properties of three of the four oligomer duplexes reported in this paper.

Sensitive proton-detected 2D-NMR assignments of ^{13}C nuclei have been applied to DNA molecules (Leupin et al., 1987; Sklenar & Bax, 1987; LaPlante et al., 1988a,b; Ashcroft et al., 1989, 1991; Varani & Tinoco, 1991; Wang, 1992). The 2D methods are complemented 1D spectral comparisons and can be used for reliably assigning the ^{13}C resonances of the bases in short nucleic acid duplexes (LaPlante et al., 1988a). This point is underscored by the fact that our laboratory has developed a computer algorithm using Bayesian statistics to assign the base carbons in oligo-DNA duplexes (Hyman et al., 1988). A casual reader of the NMR literature may not understand that "unequivocal" 2D-NMR assignment methods may fail when ^{1}H signals overlap severely (as they often do in oligonucleotides) and/or dispersion and digital resolution are too low in the ^{13}C dimension. Thus it is useful to develop comparative assignment methods at least as a backup for 2D methods. The present paper assigns the ^{13}C spectra of the deoxyribose moieties in four self-complementary oligo-DNA duplexes, using a combination of 2D proton-detected heteronuclear correlation experiments (^{1}H-{^{13}C}-COSY) and 1D spectral comparisons.

Detailed consideration of ^{13}C δ *vs* T profiles to assign the deoxyribose resonances is also useful in beginning to understand the structural changes that occur before and during duplex melting. Analysis of the δ vs T profiles is consistent with a considerable variation in the populations of the available ψ-states in the deoxyribose rings. In this study, there is a strong correlation of the changes in chemical shift with the purine/pyrimidine nature of the base attached at C1′. Eighteen of the twenty-two first-neighbor orientations of the base pairs in the four molecules are of the R–Y or Y–R type (R = purine, Y = pyrimidine), so the origin of the observed correlations may be in the relief of interstrand purine–purine steric clashes via alterations in the sugar pucker (Calladine, 1982; Dickerson, 1983). It appears that the distribution of ψ-states for the "dangling" T residue in $[d(TCGCG)]_2$ stands in sharp contrast to thymidine sugars in Watson–Crick paired residues and single-stranded DNA.

† This investigation was supported in part by National Institutes of Health Grants GM 35069 and RR 01317.

* Author to whom correspondence should be addressed.

‡ Chemistry Department, Syracuse University.

§ Present address: Biomega, Inc., 2100 rue Cunard Laval, Quebec, H7S 2G5 Canada.

‖ Present address: Departmento de Quimica, 97100 Santa Maria-RS, Brazil.

⊥ Present address: Department of Radiotherapy and Oncology, Helsinki University Central Hospital, SF-00290, Helsinki, Finland.

▽ Present address: Department of Physiology and Biophysics, University of Illinois, Urbana, IL 61801.

⊛ Abstract published in *Advance ACS Abstracts,* February 1, 1994.

[1] Abbreviations: ^{13}C, carbon-13; NMR, nuclear magnetic resonance; ^{1}H, proton; ^{1}H-{^{13}C}-COSY, proton-detected heteronuclear correlated spectroscopy; ppm, parts per million; DSS, 3-(trimethylsilyl)-1-propanesulfonic acid; δ *vs* T, chemical shift versus temperature; $\Delta\delta$, change in chemicalshift; A, adenosine; T, thymidine; G, guanosine; C, cytidine; R, purine nucleoside; Y, pyrimidine nucleoside; ψ-state, a specific envelope or twist pseudorotational state of the furanose ring (Saenger, 1984). The oligonucleotides discussed in this paper have no terminal phosphates; therefore the IUPAC notation for oligomers is abbreviated by leaving out the phosphodiester linkage.

0006-2960/94/0433-2430$04.50/0 © 1994 American Chemical Society

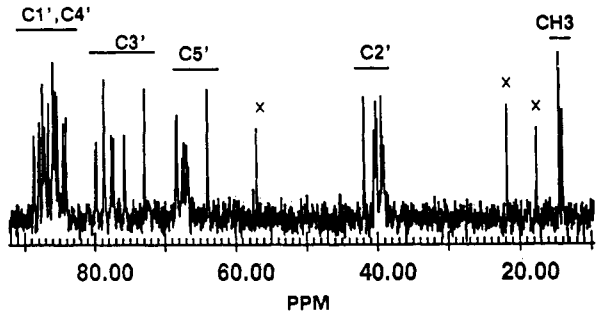

FIGURE 1: ^{13}C-NMR natural-abundance spectrum of the sugar region of [d(TAGCGCTA)]$_2$ at 125.8 MHz. × denotes peaks from DSS.

MATERIALS AND METHODS

Samples of **1** ([d(TAGCGCTA)]$_2$) and **2** ([d(GGTATACC)]$_2$) were synthesized and purified as previously described (Borer et al., 1988). Molecules **3** ([d(CGCGCG)]$_2$) and **4** ([d(TCGCG)]$_2$) were prepared by A.H.-J.W. with the collaboration of Prof. J. H. van Boom and Dr. G. A. van der Marel. One-dimensional ^{13}C spectra were acquired at 90.56 MHz (Bruker WM-360) or 125.8 MHz (General Electric GN-500). Conditions for spectra run on the WM-360 were as follows: 2-mL samples at 10–20 mM in single strands (50–100 mg) in 10-mm-diameter sample tubes; 10 000–50 000 transients were averaged with 8K × 2 data tables; 90° pulses with "Waltz" decoupling. Conditions for spectra run on the GN-500 were as follows: 0.4-mL 10–20 mM samples (10–20 mg) in 5-mm tubes; 5000–20 000 transients; 16K × 2 data tables; 90° pulses with "MLEV" decoupling. Repetition rates were 1–2 s and decoupler heating was negligible. Assignments from the ^{1}H-{^{13}C}-COSY experiments are discussed elsewhere (LaPlante et al., 1988b).

Nomenclature. In this and the accompanying paper, specific carbons are referred to with the nucleoside type designated first by letter, the chain position second, and the carbon group last. For example, G3,1′ of [d(TAGCGCTA)]$_2$ represents the deoxyribose 1′ carbon in the guanosine located at residue three, numbered from the 5′-end. The advantage of the suggested nomenclature over others involving subscripts, superscripts, or parentheses is obvious to a typist and is easily adapted for use in standard computer languages. Individual protons are not discussed in this paper, but nomenclature exemplified by G3H1′, G3C1′, and G3^{17}O4′ is recommended in cases where the nuclide is not clear from the context. TC3′ designates the "class" thymidine carbon-3′, whereas the word "group" is used to distinguish carbons at the same deoxyribose position regardless of the attached base. For example, the C3′ group includes the AC3′, CC3′, GC3′, and TC3′ classes. The terms "negative slope" and "shielding" are used interchangeably to describe a δ *vs* T profile that slopes downward (decreasing ppm) as temperature is increased; conversely, positive slopes indicate deshielding with increasing temperature.

RESULTS

^{13}C Resonance Assignments. A 1D spectrum of the sugar and T-CH$_3$ region of **1**, [d(TAGCGCTA)]$_2$, is shown in Figure 1. The C3′, C1′, and C4′ resonances of **1** and **2**, [d(GGTATACC)]$_2$, were previously assigned by the two-dimensional ^{1}H-{^{13}C}-COSY method at 25 °C (LaPlante et al., 1988b; Ashcroft et al., 1991). The assignments in **1** and **2** were then used to distinguish the C3′, C1′, and C4′ groups in **3**, [d(CG)$_3$]$_2$, and **4**, [d(TCGCG)]$_2$, by comparison of δ *vs.* T profiles while accounting for nucleoside stoichiometry and resonance multiplicity due to ^{31}P coupling.

The C5′ and C2′ profiles were not assigned by the 2D ^{1}H-{^{13}C}-COSY method, since these carbons have two attached protons and complex crosspeaks with considerable overlap and mutual cancellation. Tentative assignments of these profiles were made by 1D spectral comparisons similar to those used for assigning C3′, C1′, and C4′ of **3** and **4**. Details of the assignments are given in the Appendix. To fully appreciate the consistency of the assignments and the wealth of structural detail available in these δ *vs.* T profiles, the interested reader is urged to examine the Appendix.

The majority of assignments determined in this paper agree with those from a preliminary report (Zanatta et al., 1987). The assignment errors in that report were due to lack of sufficient data to identify the trends. For example, the ^{1}H-{^{13}C}-COSY assignments were not available and also the experiments on **1** and **4** had not been done.

δ vs T Observations. The ^{13}C profiles change dramatically and exhibit trends that have an interesting dependence on carbon group, class, and sequence. These trends correlate strongly with the base attached at C1′. The results for each carbon group are examined in the next five paragraphs.

In the C1′ group (Figure 2) most of the pyrimidine nucleoside (Y) carbons are about 2 ppm less shielded than those in the purine nucleosides (R) in the high-temperature coil form. The C1′ also stand in interesting contrast to the other sugar carbon groups (see below) in that the former have virtually no peaks with negatively sloped profiles (the dangling T1,1′ of **4** is the lone exception). It can also be seen that, on nonterminal residues, the GC1′ have similar shapes and extrema, as do the AC1′. The same can be said about the nonterminal CC1′, except for C2,1′, of **4** (panel 4 in Figure 2). However, this carbon might be expected to be somewhat similar to a terminal CC1′ since it is in a residue at the end of a block of paired bases. The TC1′ are much more variable than the others in the shapes and extrema of their δ *vs* T profiles. The profiles of the C1′ in terminal residues deviate from those of nonterminal residues in the same class. This deviation is generally larger for 5′-terminal residues than for those at the 3′-termini.

The fundamental trends for the C2′ (Figure 3) are that (i) the RC2′ tend to have small or negatively sloping profiles and (ii) the YC2′ curves show positive profiles with larger slopes. These trends are clear even though many individual assignments in the C2′ group were impossible to make. The same trends apply to the terminal residues for this group, although there are more substantial deviations in shape for the 3′-terminal profiles than for the 5′-terminal curves.

Individual assignments are easiest to make in the C3′ group (Figure 4) since there is generally less overlap of signals and the 2D ^{1}H–^{13}C correlation is usually unambiguous. For the nonterminal residues, the RC3′ have negatively sloping profiles, while the majority of the YC3′ exhibit the opposite trend in the helix melting region. The shapes of the δ *vs* T profiles for the YC3′ are highly variable. More will be said later about the interesting premelting transitions that are especially noticeable here. Naturally, the 3′-terminal C3′, lacking a phosphate, are considerably more shielded than the others. Also, the shapes of their curves are quite different from those of the C3′ in the same class at other chain positions. The 5′-terminal C3′ also exhibit unusual shapes.

Generally, the nonterminal YC4′ exhibit positively sloping profiles while the RC4′ show very small slopes (most often slightly negative) in the melting region (Figure 5). Like the

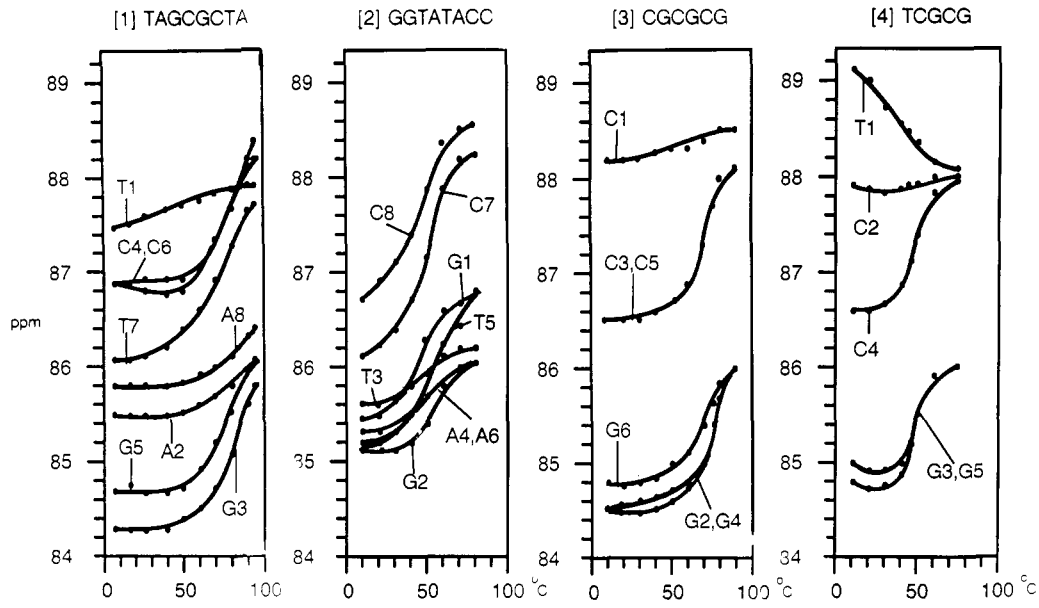

FIGURE 2: $^{13}C1'$ chemical shift *vs* temperature profiles for four DNA oligonucleotides. Note that the $^{13}C4'$ resonate in this region as well (see Figures 1 and 5).

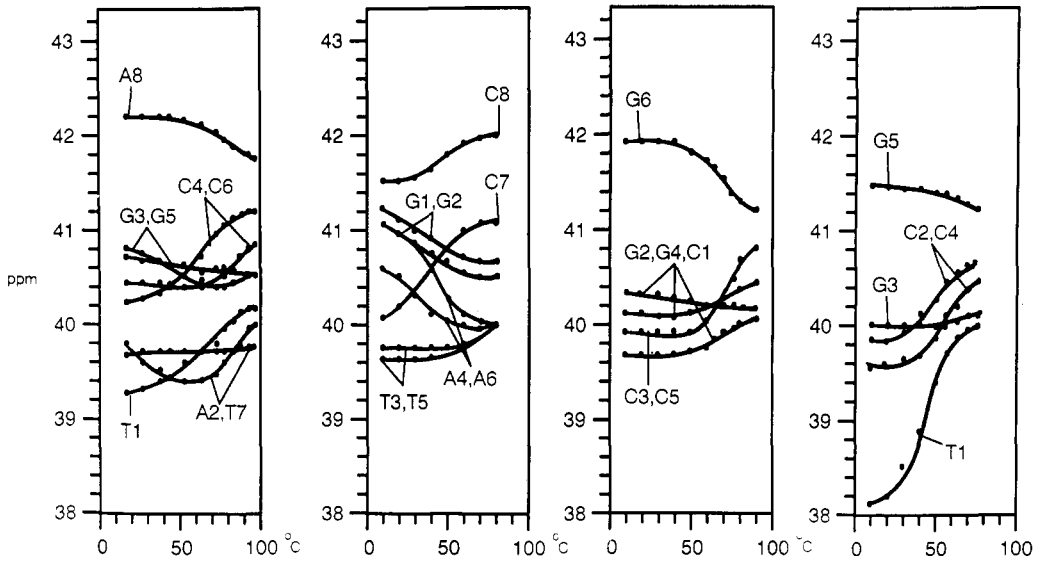

FIGURE 3: $^{13}C2'$ δ *vs* T profiles.

C3′ melting profiles, the residues at both termini have curves with unusual shapes.

Finally, the C5′ curves in Figure 6 indicate that the nonterminal RC5′ tend to have negatively sloping melting curves, with positive slopes for most of the nonterminal YC5′ in the melting region. The CC5′ transition curves have more variable shapes than most, with small $\Delta\delta$, quite in contrast to the cytidine δ *vs* T profiles for the other sugar carbons. Some premelting transitions are noticeable here, especially among the YC5′. The terminal residues show distinctly different shapes at both ends, and, of course, the lack of a phosphate dramatically shields the 5′-terminal C5′.

DISCUSSION

The key observations to be discussed are the large changes observed in chemical shift and the dependence of the shapes of the δ *vs* T profiles on the nature of the attached base—especially that the curves segregate according to the purine or pyrimidine nature of the attached base. The explanation must consider (i) alterations in deoxyribose ring torsion angles, (ii) changes in the glycosyl torsion angle, χ, and the ribose–phosphate backbone torsion angles, (iii) steric contacts, and (iv) magnetic anisotropies of neighboring bases and phosphates.

Quantum mechanical calculations (Giessner-Prettre, 1985) of the magnetic shielding constants for the deoxyribose ^{13}C nuclei indicate that large effects ($\Delta\delta$ up to 6 ppm) can be expected upon changing the sugar pucker from 2′-endo (S-form) to 3′-endo (N-form). Small changes (*ca.* 1 ppm) were calculated for rotation about the C4′–C5′ bond. Na^+ ion binding to the phosphates and the relatively large dipole moments of the C and G may also contribute through polarization of the bonding electrons, though their effects are more difficult to predict. The calculations strongly suggest that the state of the N–S equilibrium should exert the principal effect on the deoxyribose chemical shifts. Lankhorst et al. (1983), in studying ^{13}C chemical shifts of single-stranded RNA oligomers, determined that $\Delta\delta$ values as large as 5 ppm occur upon complete N–S conversion. These conclusions were verified in measurements by Stone et al. (1986) and Varani

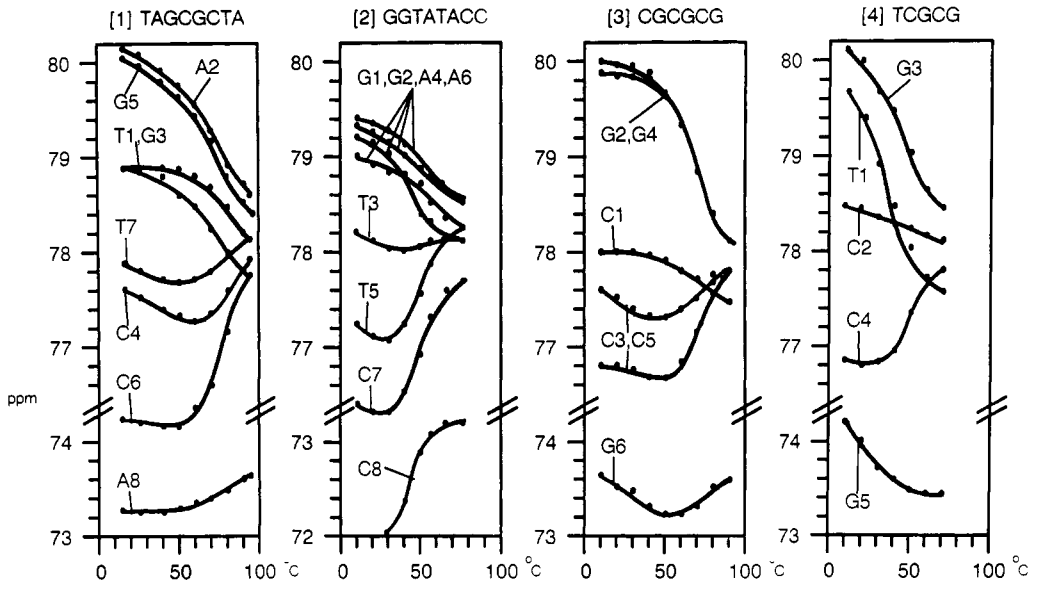

FIGURE 4: ^{13}C3′ δ *vs* T profiles.

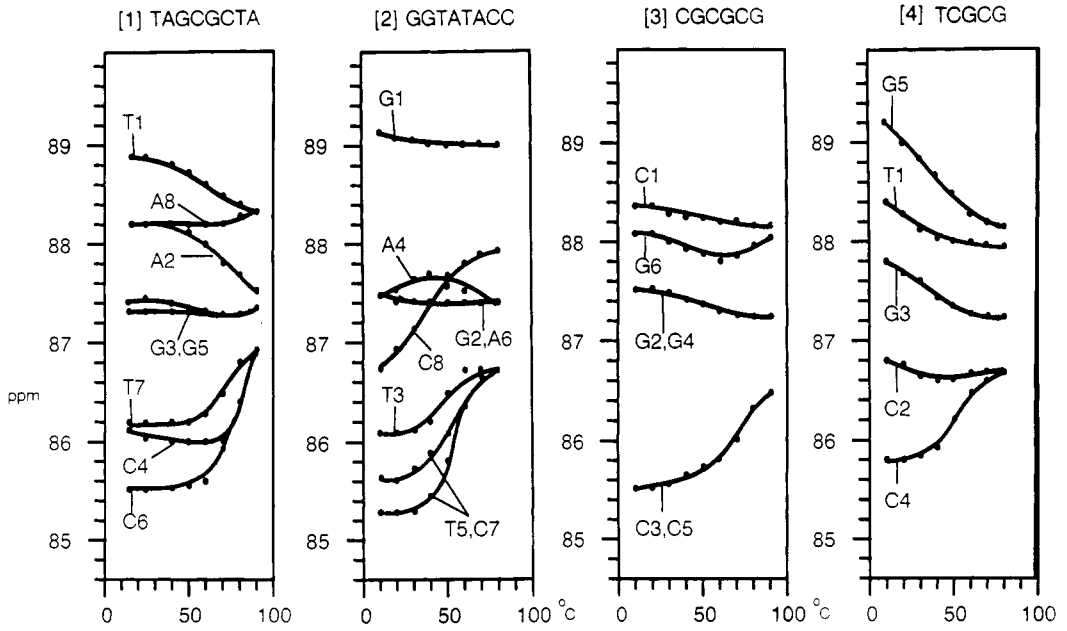

FIGURE 5: ^{13}C4′ δ *vs* T profiles. Note that the ^{13}C1′ resonate in this region as well (see Figures 1 and 2).

and Tinoco (1991). Thus the quantum mechanical calculations appear to be roughly correct. In the present study the largest $\Delta\delta$ values upon thermal dissociation of the duplexes are *ca.* 2 ppm, much larger than the changes typical in proton spectra. In considering the Giessner-Prettre and Lankhorst et al. results, a 2 ppm change would correspond to a maximum alteration of *ca.* 30% in the population of S-forms in our studies. A change of *ca.* 30% S for some residues can be inferred from ^{1}H–^{1}H COSY measurements of **1** over the 5–85 °C temperature range (Bishop, K. D., Heffron, G. J., & Borer, P. N., unpublished results). However, the varied shapes of the ^{13}C δ vs T profiles suggest that a detailed explanation will be more complex than a simple S–N conversion, as was first pointed out in our earlier work (Borer et al., 1984).

Much is already known about the configuration of the deoxyribose moiety in DNA oligomer duplexes from ^{1}H-NMR measurements in solution. ^{1}H NOE and COSY measurements indicate that the molecules have B-family DNA duplex structures with S-puckered sugars being favored (Bax & Lerner, 1988; Reid, 1987; Gronenborn & Clore, 1985; Suzuki et al., 1986; LaPlante, 1988; Patel et al., 1986; Cheng et al., 1984). Measurements of sugar proton coupling constants in a variety of DNA duplexes are especially interesting, where R-residues are usually found in S-states (>85% except for 3′-terminal sugars), while the Y-residues are 60–90% in S-forms (Altona, 1987; Rinkel & Altona, 1987; Rinkel et al., 1987a,b; Bax & Lerner, 1988; Schmitz et al., 1990, 1992, 1993; Oschkinat et al., 1987). In a single-stranded DNA, even at relatively high temperatures, the furanose rings still exhibit a substantial preference for S-forms. The energy barriers between the various ψ-states in the S-range are small, and even the barrier between S and N at O4′-endo is $\leq$5 kcal (Saenger, 1984). Thus a rapidly equilibrating blend of S and N sugar puckers should exist, with substantial populations of many of the ψ-states, especially at high temperatures. As the furanose ring moves through the available ψ-states, there are large changes in the torsion angles (70–80°), as well as alterations in bond angles and bond lengths (Saenger, 1984). The ψ-motions occur on a time scale <1 ns (Borer et al., 1994, 1984; Kearns, 1987; Zanatta et al., 1987); thus the ^{13}C

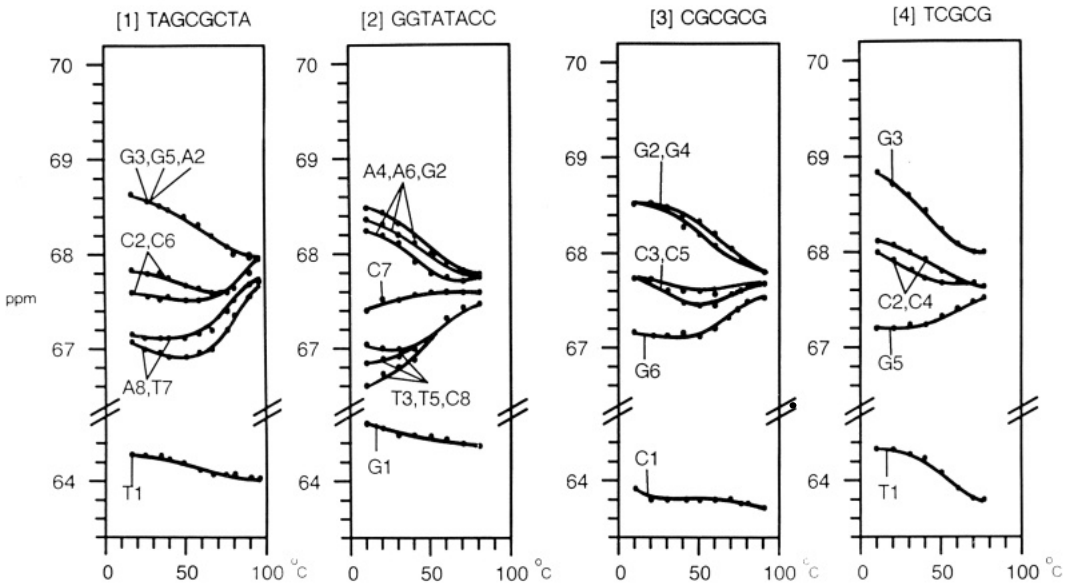

FIGURE 6: $^{13}C5'$ δ *vs* T profiles.

resonances will be averages weighted according to the populations of the various ψ-states.

Correlation of Chemical Shift with Sugar Pucker. Lankhorst et al. (1983) reported a ^{13}C-NMR study of RNA di- and trinucleotides that suggested a correlation between ^{13}C chemical shift and sugar pucker. ^{13}C spectra were observed as a function of temperature, and the % N conformation was determined by ^{1}H-NMR. Plots of ^{13}C chemical shifts *vs* % N sugar conformation had nearly linear correlations at each ribose carbon, although the C2′ plot had a very small slope indicating a relatively insensitive response. This suggested that the chemical shifts of the furanose ^{13}C nuclei are determined mainly by the distribution of ψ-states. The small deviations that arose were attributed to other conformational properties such as variation of the glycosyl torsion angle, χ, between the molecules and/or subtle differences in the backbone angles.

A comparison of the changes in ^{13}C chemical shift upon unstacking is made between the present DNA study and RNA dimers and trimers in Figure 7. The panels in Figure 7 are organized by sugar carbon group with C1′ in (a), C2′ in (b), etc. The "front" series, S1, shows the average of the $\Delta\delta$ ($\delta_{hiT} - \delta_{loT}$) values for **1**, **2**, **3**, and **4**, series S2 shows the average $\Delta\delta$ ($\delta_{hiT} - \delta_{loT}$) of RNA trimers from Stone et al. (1986) (no C-containing oligomers were studied), and series S3 shows the average $\Delta\delta/3$ ($(\delta_{100\%S} - \delta_{100\%N})/3$) of RNA dimers and trimers extrapolated from the Lankhorst et al. (1983) data (no C- or G-containing oligomers were studied). The RNA averages have the bars all pointing the same direction within the C1′ group, as well as within the C3′, C4′, and C5′ groups. This reinforces the idea that the ^{13}C chemical shifts respond in a predictable way to changes in the sugar puckering equilibrium. (The very small positive $\Delta\delta$ values for AC2′ are the only exception to this general trend.) There is no dramatic variation that depends on the R/Y nature of the base for these RNA single strands.

Similar results were found by Varani & Tinoco (1991) on an RNA hairpin of 12 residues. The conformation of the molecule in solution has been analyzed by measurements of ^{1}H–^{1}H NOEs as well as ^{1}H–^{1}H and ^{1}H–^{31}P coupling constants (Cheong et al., 1990; Varani et al., 1991). While several of the furanose rings adopt the usual N-forms for RNA duplexes, two of the loop Y-nucleosides are in the S-form, and one

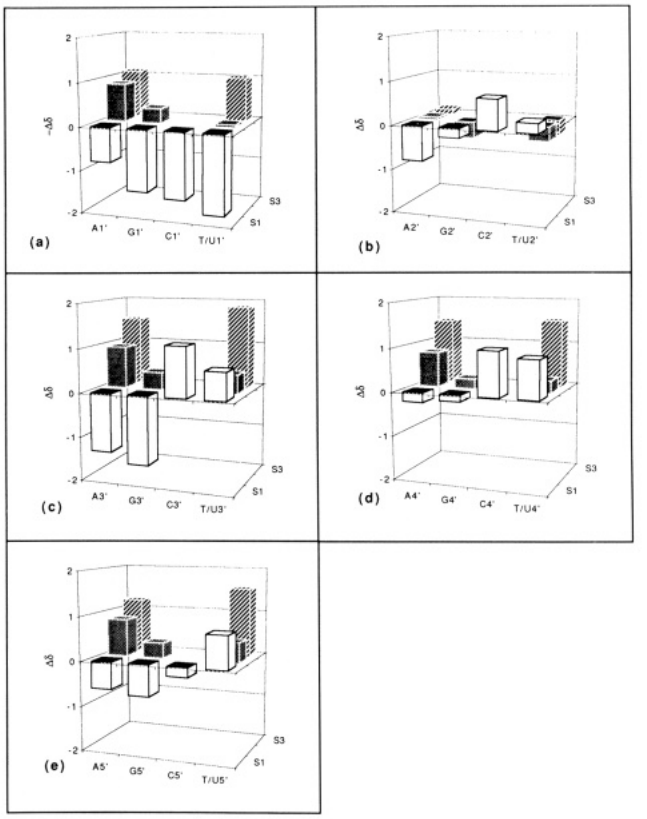

FIGURE 7: Average ^{13}C $\Delta\delta$ for the sugar carbon classes of DNA (S1 for A, G, C, and T from this study, $\Delta\delta = \delta(85°) - \delta(10°)$) and single-stranded RNA (S2 for A, U, and G only from Stone et al. (1986), $\Delta\delta = \delta(70°) - \delta(11)°$, and S3 for A and U only from Lankhorst et al. (1983), $\Delta\delta/3 = (\delta(100\%\ S) - \delta(100\%\ N))/3$). The panels show (a) C1′ (vertical axis is $-\Delta\delta$), (b) C2′, (c) C3′, (d) C4′, and (e) C5′.

R-residue has an unusual *syn* orientation about the glycosyl bond. The differences between the mean values of the ^{13}C chemical shifts for S- and N-forms correlated very well with the Lankhorst et al. (1983) predictions.

However, the $\Delta\delta$ values of the deoxyribose rings in the present DNA study show a much more varied response; the DNA R- and Y-nucleosides exhibit opposite signs for most of the $\Delta\delta$ except C1′ (series S1 in Figure 7b–e; the special character of the C1′ $\Delta\delta$ values will be considered later in the

section Effect of Changing χ). Can the differences in the DNA and RNA characteristics be reconciled with the Altona/Lankhorst hypothesis that changes in the populations of the ψ-states are the primary determinant of the observed δ values for the sugar carbons?

The sugar pucker equilibrium in A-family duplexes and in stacked single-stranded RNA is dominated by N-forms, and destacking causes an increase in the % S. Thus, in a simple two-state puckering model, bars with the same sign as the RNA trend in Figure 7 should correspond to an increase in S-states upon destacking (increasing temperature). The usual expectation is that the deoxyribose rings in DNA will shift toward a higher population of N-forms upon duplex melting. In that case the signs of the DNA bars in Figure 7 should anticorrelate with the RNA bars; this does occur for the R-sugars (except C2′), while the correlation is clearly mixed for the Y-sugars (only five of the ten bars anticorrelate with the RNA trend).

A comprehensive theory for the trends in the ^{13}C chemical shift changes in the sugars upon melting DNA still requires further study. However, the rest of this section discusses published and unpublished work that may be useful. There is an extensive body of published work on the conformational analysis of DNA sugars from analyzing ^{1}H–^{1}H coupling constants and NOEs, as well as X-ray diffraction data. A comprehensive review is beyond the scope of this paper, and the subject is highly controversial. Most of the studies agree that the sugar ring is highly flexible and that the populations of the various conformers are influenced by sequence effects. Three classes of interpretation will be considered in the following order: (i) that two ψ-states are sufficient to describe the sugar pucker equilibrium at each residue, (ii) that three or more discrete conformers may be substantially populated in some residues, and (iii) that accessible ψ-states vary in a nearly continuous fashion around much of the pseudorotation cycle with the distribution skewed by sequence effects. A prototype for the latter was the proposal that 5 furanose conformers in the range of $100° < P < 150°$ can be populated in response to steric clashes between purines on opposite strands [Calladine, 1982; Dickerson, 1983; see also Saenger (1984); P is the pseudorotation phase angle].

(i) Altona and co-workers developed a two-state approximation to estimate the variation in % S and ψ-state for the sugars in DNA duplexes and single-stranded monomers from measurements of sugar ^{1}H–^{1}H coupling constants (Rinkel & Altona, 1987). They usually assume a minor N-form with a fixed conformation in fast equilibrium with a *single* major S-conformer and then determine the parameters % S as well as P and ϕ_{max} for the S-conformer (P is the pseudorotation phase angle; ϕ_{max}, the maximum amplitude of pseudorotation, is relatively unimportant[2]). Any of the endocyclic torsion angles can be calculated from P and ϕ_{max}, with the C5′–C4′–C3′–O3′ backbone torsion angle, δ, being of special interest (see eq 3, Rinkel et al., 1987b). Of course, if the distribution of δ-angles changes, the other torsion angles in that furanose must change as well, as this will affect the chemical shifts of all of the ring ^{13}C nuclei. The Altona two-state approximation has been applied by a number of other groups as well, and the general conclusions are similar to those reported in a series of papers on four duplexes and the temperature dependence of four monomeric strands (Rinkel et al., 1987a,b; Orbons et al., 1987).

Table 1: Two-State Modeling of the Sugar Pucker Equilibrium for R- and Y-Residues in DNA Duplexes and Single-Stranded Monomers for Non-3′-terminal Residues[a]

	% S[b]	δ[c] (deg)	N[d]
R-duplex[e]	90 ± 7	144 ± 3	9
R-duplex, YRY[e]	85 ± 8	146 ± 2	3
R-monomer[e,f]	91 ± 7	146 ± 4	5
R-monomer Δ% S(10–85 °C)[f]	13 ± 5	ND[g]	5
Y-duplex[e]	80 ± 10	135 ± 13	12
Y-duplex, RYR[e]	82 ± 10	121 ± 8	4
Y-monomer[e,f]	79 ± 5	140 ± 2	7
Y-monomer Δ% S(10–85 °C)[f]	6 ± 5	ND[g]	7

[a] Data for duplexes ($[d(CACATGTG)]_2$ and $d[(GAGATCTC)]_2$) and monomers (d(CACA), d(TGTG), d(GAGA), and d(TCTC)) are from Rinkel et al. (1987b), data for $[d(CCGAATTCGG)]_2$ are from Rinkel et al. (1987a), and data for $[d(m^5CGm^5CGAGm^5CG)]_2$ are from Orbons et al. (1987; residues from the central G:A mismatch were not used to generate the averages in the table). [b] Average % S and standard deviation. [c] Average δ-torsion angle for major S-conformer and standard deviation. [d] Number of residues used in calculating the averages and standard deviations. [e] Temperature ~25 °C; see note *f* for the temperatures used to estimate % S at 25 °C for the monomers. [f] Temperatures for the monomer measurements were 25, 34, and 57 °C for d(CACA), 10, 24, and 33 °C for d(TGTG), 19, 34, and 47 °C for d(GAGA), and 2, 14, 35, and 47 °C for d(TCTC); values of % S were estimated at 10, 25, and 85 °C from the linear regression coefficients. The trend is to decrease % S upon increasing temperature. [g] ND = not determined; the same δ-torsion was assumed for each temperature.

Table 1 provides a summary of these results, ignoring data from residues at the 3′-end of each strand (which has an abnormally high fraction of the N-form in most DNA molecules). On average, the R-sugars are *ca.* 90% S, whereas the Y-sugars are *ca.* 80% S in either duplexed or monomeric chains. The statistical sample for alternating RY sequences is not large, but ~85% S characterized both R- and Y-sugars in the duplexed sequence: $[d(CACATGTG)]_2$. It appears that % S(R) in monomeric strands has about twice the temperature dependence as % S(Y), with both in the ~75–80% range at higher temperatures. Thus, a practical upper limit on the change in % S induced by thermal strand dissociation is 25%, with that for alternating RY sequences being ~5–10%. In addition to a preference for ~90% S, the R-sugars have δ_{exp} values clustered tightly around 145°, insignificantly different from the values measured for δ(R) in stacked, single-stranded oligomers. Notice that the standard deviations about the mean values are <5°. While the R-sugars respond to increasing temperature by decreasing % S, the Y-sugars appear to respond to altering δ. Perhaps the most conspicuous trend in Table 1 relates to the large variation for δ(Y) in the duplexes (~25°) depending on the sequence context; the mean δ(Y) tends to be *ca.* 10° less than δ(R) in duplexes and is most exaggerated in alternating RY sequences. However, in monomeric strands, average δ(Y) increases toward the average δ(R) value, and the standard deviation becomes only a few degrees.

The just-described application of the two-state model can be used to rationalize the averaged ^{13}C chemical shift measurements shown in Figure 7. Upon duplex melting, substantial S to N changes for the R-sugars should be expected and the signs of the chemical shift changes are opposite to the N to S transitions occurring for RNA; there should be very little change due to small alterations in δ-angle for the single S-conformer. However, for the Y-sugars a much smaller increase in N states should be accompanied by more strongly sequence-dependent changes in δ-angle; these two effects may

[2] Using a constant value of $\phi_{max} = 38°$ usually introduces less than a 5° error in converting P to δ. The error is largest for $0° < P < 70°$ (in the N-range; $\delta \sim 90°$) and $180° < P < 250°$ (in the high S-range; $\delta \sim 160°$); neither region is of much interest for DNA oligomers, where most observations place $120° < \delta < 150°$, and the P to δ conversion errors are 0–3° using $\phi_{max} = 38°$.

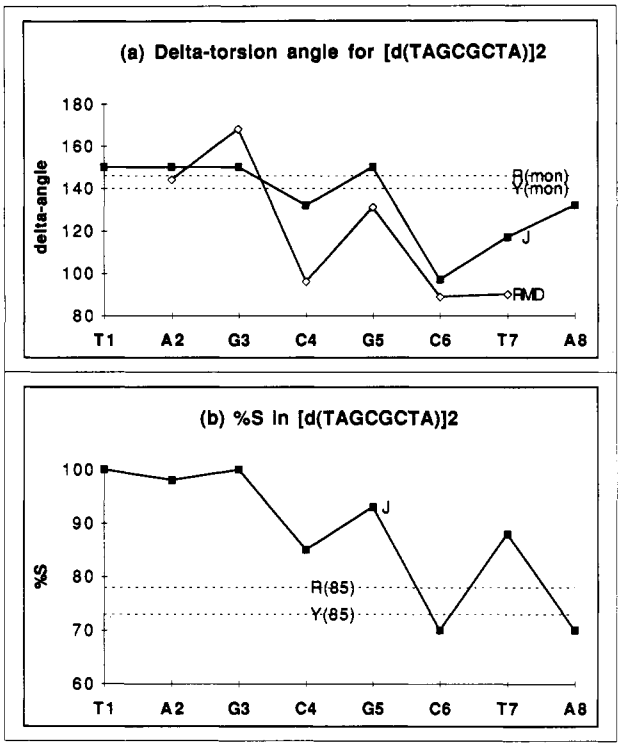

FIGURE 8: Variation in (a) δ-angle and (b) % S in $[d(TAGCGCTA)]_2$ from analyzing 2D ^1H–^1H COSY and NOE spectra. (a) The line labeled "J" used the sugar coupling constants as input. The line labeled RMD used distance-restrained molecular dynamics interpretations of the NOE intensities (AMBER). (The RMD calculations do not correct for % S or use torsional restraints, therefore it would be surprising if they agreed exactly with the δ-angle determined by *J* coupling. However, the qualitative trends are reproduced. The RMD results give highly variable results for the terminal residues, so they are not shown.) The dashed lines show the expectations for R- and Y-nucleosides in monomeric strands (lines 3 and 7 from Table 1), which should be close to the δ-angles upon strand melting. (b) The line labeled "J" used the sugar coupling constants as input, and the dashed lines should be near the % S values for R- or Y-sugars in monomeric strands at 85 °C (lines 3 and 4 and lines 7 and 8 from Table 1).

balance, making it problematic to predict the sign of the chemical shift change. It would be expected that the chemical shift changes on increasing the δ-angle from ~120° (typical of Y in RYR sequence duplexes; see Table 1) to the monomer strand value of ~140° would be the same direction as the N ($\delta \sim 90°$) to S ($\delta > 120°$) transition for RNA. Panels e and d Figure 7, illustrate exactly this result for the $^{13}C3'$ and $^{13}C4'$ chemical shifts, and these are the carbons for which alterations in electronic structure would be most strongly affected by changes in the δ-angle.

Average changes help to relate the general trends in chemical shifts to average changes in the distribution of ψ-states. However, knowledge of the equilibrium for specific molecules is required for a detailed understanding of the chemical shift effects. Figure 8 shows results (Wang, Y., Kerwood, D., Borer, P. N., unpublished results) for **1** obtained by analyzing 2D ^1H–^1H-COSY and NOE spectra. Figure 8a shows results of calculations of δ-angles according to the method of Rinkel and Altona (1987) using the sugar coupling constants as input (square symbols) and using distance-restrained molecular dynamics interpretations of the NOE intensities [diamond symbols; the RMD calculations were done in a similar manner to that described by Schmitz et al. (1992), without incorporating torsional restraints]. The dashed lines show the expectations for R- and Y-nucleosides in monomeric strands (see Table 1), which should be close to the δ-angles upon strand melting. Likewise, Figure 8b shows results of calculating % S from coupling measurements (Rinkel & Altona, 1987), and the dashed lines should be near the % S values for R- or Y-sugars in monomeric strands at 85 °C (Table 1). There is good qualitative agreement regarding the trends in δ-angle determined from *J*-coupling and RMD, with the smallest values occurring for residues C6, C4, and T7 (we shall ignore the 3′-terminal A8 in this discussion); relatively larger δ-angles (and % S) are observed for T1, A2, G3, and G5. Now return to the first panel of Figure 4 ($^{13}C3'$) and of Figure 5 ($^{13}C4'$). The profiles with negative slopes are T1, A2, G3, and G5 and those with positive slopes are C6, C4, and T7, exactly as would be predicted from the preceding discussion. T1, A2, G3, and G5 apparently undergo sizable decreases in % S upon strand melting, while C6, C4, and T7 already have low % S and melting skews the distribution of ψ-states toward larger δ-angles. This interpretation rationalizes two other curious and sequence-specific facts: first, T1 is a pyrimidine nucleoside but exhibits the chemical shift profiles of a purine (relatively large decrease in % S and little change expected in δ-angle) and, second, C6 exhibits larger positive profiles than C4 (C6 should have the largest increase in δ-angle). This new interpretation is promising, but preliminary, and should be regarded with caution until further work is done. It also begs for a structural explanation of the sequence-dependent effects, which item iii, below, begins to address.

(ii) A simple two-state model may not accurately describe the sugar puckering equilibrium. In recent work, Schmitz et al. (1992, 1993) reported structural studies of d(GTATAATG):d(CATTATAC) using molecular dynamics with time-averaged distance restraints. While they usually find a minor form in the low N-range, there can be more than one distinct conformer per residue in the S-range. The distribution of the S-forms varies substantially from one residue to another. It is too soon to judge whether this work will reveal correlations in the distribution of ψ-states with the R/Y nature of the attached base or the sequence context, or even if the modeling is sufficiently robust to accurately estimate the populations of two or more sugar conformers per residue.

(iii) It seems likely that the δ-angle in the Altona two-state model actually describes an ensemble average of S-forms, rather than a specific state where the δ-angle varies in a continuous, non-jump-like fashion. In the range from $90° < \delta < 160°$ ($80° < P < 200°$) there are four envelope ψ-states ($^{O}E, {}_1E, {}^2E, {}_3E$; Saenger, 1984) separated by 15–25° increments in δ-angle. If these are substantially lower in energy than the twist and other intermediate forms, the δ-angle should undergo discrete jumps. Then a reasonably successful two-state model, with a continuously varying δ-angle, actually reflects the average properties of the distribution of discrete microstates.

An intriguing possibility for the origin of sequence-specific values for δ-angle and ^{13}C chemical shifts is the relief of steric clashes between purines on opposite strands in the duplexes. One mode by which it has been suggested that clashes may be relieved is to increase the δ-angle for R-nucleosides and decrease it for Y-nucleosides (Calladine, 1982; Dickerson, 1983; Saenger, 1984). The strongest clashes were predicted for alternating RY sequences. However, only the most simplistic mechanical model would insist on exact compensation in δ-angles; oligomer helices in solution can also bend or alter in helix winding to compensate for a change in one equilibrium δ-angle near the site of a purine–purine clash. Rinkel et al. (1987b), in the study of $[d(CACATGTG)]_2$ discussed above, noted that the primary changes were large

decreases in δ-angle for the Y-sugars in this alternating RY sequence while very little change was seen for the R-sugars. Similar results are seen in Figure 8a for central four base pairs in $[d(TAGCGCTA)]_2$.

The simplest rules to account for structural variation in DNA due to interstrand purine–purine clashes in the minor or major grooves were introduced by Calladine and Dickerson (Calladine, 1982; Dickerson, 1983). These rules have since been shown to be inadequate to account for sequence-dependent structural variation in crystal structures of DNA (Yanagi et al., 1991). However, it is likely that cross-strand purine clashes do occur, even though relief of these clashes probably does not follow the simple rules originally set forth. Since the clashes are probably present, it may be useful to look at the $\sum_3$ rule for B-family DNA, which predicts variation in δ-angle for the four molecules in this study (Dickerson, 1983):

1	5′-T	A	G	C	G	C	T	A-3′
	-2	+2	+1	−3	+3	−1	−2	+2
2	G	G	T	A	T	A	C	C
	0	+1	−3	+3	−3	+3	−1	0
3			C	G	C	G	C	G
			−2	+3	−3	+3	−3	+2
4				T	C	G	C	G
				?	−2	+3	−3	+2

where the numbers denote the increment in δ-angle away from the mean value. The average $\sum_3$ value is +2.2 for the R-sugars and −2.2 for the Y-sugars, predicting changes in δ-angle in opposite directions for the purine and pyrimidine residues, as reflected in the present ^{13}C data (Figure 7b–e). As was noted in the discussion in section i, above, one must also account for alterations in % S.

Other Chemical Shift Influences. Saenger (1984) notes X-ray studies showing that the endocyclic torsion angles are all highly correlated in nucleosides and oligonucleotides. Aside from the C3′ and C4′, just discussed, the endocyclic carbons are C2′ and C1′. The C2′ for the DNA R- and Y-sugars show opposite temperature dependence (Figure 7b), as expected if the ψ-state equilibrium differs in these DNA oligomers. C2′ in RNA has a hydroxyl group attached, so some difference in its chemical shift dependence might be expected. Even so, G2′ shows the only violation of the DNA/RNA trend seen for the C3′ and C4′. Further, the slope of the Lankhorst et al. (1983) chemical shift *vs* % N curves for C2′ is much smaller than for the other sugar carbons. Thus, C2′ chemical shift changes may be more susceptible to anisotropic effects of the bases than the other sugar carbons.

Saenger's (1984) collection of extant X-ray studies shows that while the endocylic torsion angles correlate very closely, γ (the angle about C5′–C4′) correlates less well than the endocyclic angles. About half of the CC5′ chemical shift *vs* *T* profiles are positive and half negative (Figure 6). The lack of a strict correlation at C5′ between R/Y character and the sign of Δδ (Figure 7e) may occur because C5′ is an exocyclic atom.

Effect of Changing χ. Unlike the other carbon groups, the C1′ profiles exhibit only positive slopes, usually accompanying large changes in ^{13}C chemical shift (Figures 2 and 7; only T1,1′ of **4** exhibits a negative slope). Also, the C1′ chemical shifts are generally larger for the Y-sugars at high temperatures than for the R-sugars (Figure 2). While changes in the equilibrium array of ψ-states must affect C1′, there are other effects that may be more important for C1′. Saenger (1984) has compiled data on crystalline mononucleosides that are useful in the following three ways for rationalizing the observed C1′ chemical shifts: (i) The glycosyl bond is 1% longer for the N-form than for the S-form. Thus, if % S decreases for the oligo-DNA residues upon duplex melting, one expects the glycosyl bonds to increase in length. This should decrease the electron density at C1′ upon duplex melting, deshielding it exactly as observed. (ii) Steric contact between the Y-base O2 or the R-base N3 and the sugar–phosphate backbone (primarily O4′) provides a barrier to *anti*/*syn* conversion, with the strongest clashes occurring for the Y-nucleosides. According to the X-ray studies, the glycosyl bond length for Y-nucleosides increases *ca* 3% upon *anti* to *syn* conversion, whereas the C1′–N9 distance remains nearly constant in R-nucleosides. One expects some lengthening of the average C1′–N9 bond length in R-nucleosides as well, due to the steric clash. The population of *syn* states should increase as the duplex melts, so this would also deshield C1′. (iii) The X-ray studies indicate that the C1′–N bond length for R-nucleosides averages *ca.* 2% less than for Y-nucleosides. This is consistent with our observation that the ^{13}C chemical shifts of the RC1′ are *ca.* 2 ppm more shielded that the YC1′ at high temperatures (Figure 2).

Steric Clashes. Changes in the endocyclic, backbone, and glycosyl torsion angles are likely to generate close contacts between atoms. There is ample precedent for steric effects on the chemical shifts of carbon nuclei (Siedman & Maciel, 1977; Winstein et al., 1965; Levy & Nelson, 1974; Stone et al., 1986; LaPlante et al., 1988a). While these effects can be quite large (5 ppm) in small organic compounds where rigid structures force atoms into strong steric conflict, the DNA backbone is probably sufficiently flexible and mobile to prevent really bad contacts. However, the introduction of *syn* states at high temperatures could result in steric contact effects, particularly at C3′ in N-states and (less severely) for C2′ in S-states.

Premelting. Several of the profiles, especially among the C3′ (Figure 4) exhibit substantial changes in chemical shift prior to the onset of helix melting. These changes are almost certainly due to redistribution of the ψ-states in the duplex that lead to changes in average torsion angles in the sugar–phosphate backbone. If a major source of the differences in ^{13}C chemical shift in each of the sugar carbon groups is the relief of interstrand purine clashes, there could be temperature-dependent changes in the blend of microstates in the duplex. Note in Figure 4 that C4,3′ and C6,3′ in **1** exhibit substantial premelting transitions. Changes in χ could also produce changes in ^{13}C chemical shifts, through steric and polarization effects.

A Dynamic DNA Duplex. The value of an equilibrium "structure" for a DNA duplex is called into question if a distribution of ψ-states is populated at many of the sugar moieties. This is even more a concern if the distribution changes with temperature (and perhaps ionic environment) as it apparently does. If these concerns are shown to be valid by further experiments, there are some important consequences. First, structures from interproton NOE and X-ray diffraction studies are likely to disagree at some level since they result from different averages over the microstates. For instance, the position of H2′ changes by *ca.* 1 Å with respect to the C4′–O4′–C1′ plane in the S to N transition (^{2}E to ^{3}E); furthermore, the δ-torsion angle can change by *ca.* 60° while the furanose stays completely within the S-range (Saenger, 1984). Changes in furanose pucker will be accompanied by concerted motions in other parts of the sugar–phosphate

backbone as well, although the ensemble-averaged structure probably does not change as dramatically as in the B to A transition, for example. Second, and perhaps more importantly, an understanding of the time scales and amplitudes of local motion may be required to relate biological function to the sequence-dependent physical properties of DNA. In separate work (Borer et al., 1994, 1984; Zanatta et al., 1987), we have measured the relaxation properties of **2**, **3**, and **4** and find that the ^{13}C–^{1}H T_1 and NOE values are larger for the sugar than the base carbons. Careful analysis of the data suggests that the average amplitude of the motion is substantially larger for the sugars ($S^2 \simeq 0.6$; $\theta_w > 30°$) than for the bases ($S^2 \simeq 0.8$; $\theta_w \simeq 20°$; Borer et al., 1994). The time scales are more difficult to define accurately from the relaxation data, although it is clear that the sugar motions must occur on the subnanosecond scale, with internal correlation times in the 100-ps range (Borer et al., 1994).

The Special Case of the "Dangling" T-Residue. The 5′-dangling T residue in **4** has very unusual melting profiles for its sugar carbons. T1,1′ (Figure 2, panel 4) is the only C1′ profile exhibiting a negative slope. In view of the earlier discussion, this suggests that χ may be constrained to an unusual average value for this residue in the duplex state. The T1,2′ (Figure 3, panel 4) exhibits a $\Delta\delta$ of almost 2 ppm, while the change is much smaller for most of the other C2′. Likewise, $\Delta\delta = -2.2$ ppm for T1,3′ is clearly atypical for a 3′-carbon (see Figure 4); this change is larger than that seen for all of the other carbons in the study. The trend for T1,4′ and T1,5′ (panel 4, Figures 5 and 6) is toward negative $\Delta\delta$, again in contrast with the positive $\Delta\delta$ seen in nonterminal T-residues. In single-stranded CT_3GT_3G, the temperature-dependent $|\Delta\delta| \leq 0.2$ ppm for all of the T carbons (Boudreau, 1992), so T1 in $[d(TCGCG)]_2$ is apparently constrained to an unusual distribution of microstates that bears very little resemblance to "single-stranded" DNA. Further study of this and similar molecules may yield important insights into the junctions between base-paired and unpaired regions in DNA.

CONCLUSION

Natural-abundance ^{13}C-NMR spectra of DNA oligonucleotides are readily measured, and methods are available for the nearly complete ^{13}C resonance assignments of the deoxyribose moieties of DNA oligonucleotides. Measurements of δ *vs* T profiles are consistent with the following: (i) the sugar pucker is a main determinant of the sugar carbon chemical shifts; (ii) the distribution of ψ-states correlates strongly with the purine/pyrimidine character of the attached base, at least in sequences with alternating purines and pyrimidines; (iii) there are substantial changes in the distribution of ψ-states and possibly glycosyl and backbone torsion angles in the premelting regions; (iv) the ensemble-average configuration of the T-sugar in $[d(TCGCG)]_2$ is very different from a single-stranded or Watson–Crick paired T.

ACKNOWLEDGMENT

The authors are grateful for helpful discussions with Profs. G. C. Levy and Istvan Pelczer. The NMR1 and NMR2 software packages were used to process spectra (Tripos Associates, St. Louis, MO).

APPENDIX: DETAILED ^{13}C ASSIGNMENTS

C3′ Assignments. These are the simplest since their resonances are quite widely dispersed in all four duplexes and their ^{1}H–^{13}C correlation is generally unambiguous (LaPlante et al., 1988b). From the assignments in **1** and **2** (left two panels of Figure 4) it can be seen that the YC3′ are more shielded than the RC3′ in the low-temperature duplex and exhibit opposite slopes in the duplex melting region. T1,3′ and A8,3′ in **1** violate the trends just described, but exceptions to general rules in chemical shift are often observed for carbons on terminal residues (Borer et al., 1984; LaPlante et al., 1988a). Leupin et al. (1987) observed the same relative purine/pyrimidine chemical shifts in $[d(GCATGC)]_2$, although they have not reported the temperature dependence.

It is easy to extend these unambiguous assignments to **3** (third panel of Figure 4). Here the highly shielded singlet is clearly G6,3′. Two curves slope down strongly and must be from the nonterminal G3′ by comparison with the first two panels. Two other curves have substantial positive slopes, most similar to the nonterminal cytidine-C3′ profiles in the previous panels, and are thus assigned to C3,3′ and C5,3′ in **3**. The assignment of C1,3′ as indicated in the third panel is consistent with a δ *vs* T profile from a terminal residue; i.e., its profile is dissimilar to either the Y or R category.

In panel 4, the curve labeled G5,3′ of **4** is clearly from the 3′-terminal residue since it is a singlet resonance. The curves labeled C4 and G3 are easily justified by comparison with the other figures. However, the T1 and C2 assignments are more difficult to rationalize and must be regarded as tentative. The current assignment is favored because of the following: (i) C4,3′ in **1** and either C3,3′ or C5,3′ in **3** exhibit small slopes for internal CC3′—thus a sequence-dependent change in chemical environment could produce a profile with a small negative slope; (ii) C1,3′ in **3** displays a similar profile to the curve designated as C2,3′ in **4** and both residues are at the 5′-end of a base-paired block; (iii) the T1 profiles in **1** and **4** are most similar.

C1′ Assignments. The C1′ and C4′ profiles in Figures 2 and 5 occur in the same spectral region (see Figure 1). The C1′ are all singlets, whereas the C4′ are multiplets; thus it is easy to distinguish the two carbon groups.

The unequivocally assigned C1′ signals of **1** and **2** reach high-temperature limits near 86 ppm for A and G, with the C profiles ending near 88 ppm, while the TC1′ terminate over a much wider range in temperature. The GC1′ profiles in **3** and **4** (Figure 2) are easily assigned by similarity with the first two panels since there are no interfering AC1′. Given the current data, it is not possible to make unique GC1′ assignments in **3** and **4**, except for the tentative G6,1′ in **3** since it is different from the other two G curves. Also, the logical assignment of the C1,1′ in **3** distinguishes its profile from the superimposed internal C3,1′ and C5,1′ curves. C4,1′ in **4** is in a nearly identical environment to C3,1′ and C5,1′ in **3** and C4,1′ in **1**; thus its assignment is obvious. C3,1′ in **4** is at the 5′-end of the base-paired block and is assigned to the curve most similar to C1,1′ in **3**, in a similar sequence environment.

C4′ Assignment. Due to ^{31}P coupling, the terminal C4′ signals are doublets, while the nonterminal C4′ resonate as doublets of doublets. The terminal C4′ doublets are easy to follow in all four molecules and become the least shielded C4′ in each at high temperature (Figure 5). The profiles for C1,4′ and G6,4′ in **3** and T1,4′ and G5,4′ in **4** are tentatively assigned based on the observation that the C4′ of the 5′-terminal residue resonates at lowest field in **1** and **2**. The internal GC4′ and CC4′ curves occupy distinct domains of chemical shift in **1** and **2**, so the class assignments for **3** and **4** are easily justified. The unique assignment for the curve labeled C4 in the last panel of Figure 5 can be rationalized since an internal residue (C4,4′) should be most similar to the internal CC4′ in the

other duplexes; the C2,4′ curve (labeled C2) is from a carbon at the end of the base-paired block in TCGCG.

C5′ Assignments. The C5′ profiles were all assigned by 1D spectral comparisons since assignments by the ^{1}H-{^{13}C}-COSY method were not available. First, the 5′-terminal resonances can easily be identified since they are singlets (all others are doublets) and in addition they are shifted far upfield. The similarity in sequence and nucleoside stoichiometry provides a unique opportunity to assign the C and G profiles of **3** and **4**. In comparing the profiles of **3** and **4** (see Figure 6), it is apparent that there is an additional negatively sloping profile in **3** which is downfield. Therefore the downfield profiles with similar negative slopes in both **3** and **4** are assigned to the nonterminal G nucleosides. That observation leaves three profiles unassigned in **3** and **4**. The two having small slopes and similar chemical shifts are assigned to the two nonterminal C nucleosides, and the last profile must be assigned to the 3′-terminal G by considering the stoichiometry.

The C5′ group assignments for **1** and **2** can be easily inferred from the assignments of **3** and **4**, just discussed. In **1**, three C5′ signals are superimposed over the whole temperature range (Figure 6, top left). The shape and placement of this curve are very similar to the internal GC5′ profiles for **3** and **4**, which have similar G/C sequences. Therefore, two of the three superimposed curves must originate from G3,5′ and G5,5′. Duplex **1** has only one internal A residue, while **2** has two internal A's and only one internal G. Thus the negatively sloping curves in Figure 6 (top) must correspond to G3,5′, G5,5′, and A2,5′ of **1** and A4,5′, A6,5′, and G2,5′ of **2** in their respective panels. There remain four curves in each panel to identify. The CC5′ in **3** and **4** had gently sloping profiles, and there are two closely related curves assigned to C4,5′ and C6,5′ in **1** and one related curve assigned to C7,5′ in **2** for the internal cytidines (Figure 6). That leaves the two remaining curves in **1** as A8,5′ and T7,5′ and the three remaining curves in **2** as T3,5′, T5,5′, and C8,5′. The internal consistency of the 5′-carbon class assignments in the four duplexes is clear, although it is not possible to identify many profiles with the unique carbons.

C2′ Assignments. This group is difficult to assign due to the high degree of spectral overlap; therefore these assignments must be regarded as tentative.

The curves at the top of the Figure 3 are all from singlet resonances, so they are clearly from the 3′-terminal residue in each molecule; the other signals are all doublets with coupling constants <3 Hz. In **3**, there are only GC2′ and CC2′, so the T1,2′ curve in **4** is easily distinguished. Also, in **4** there are two nearly parallel curves and one that is relatively flat. The most logical assignment is that the flatter curve belongs to G3,2′ and the other two to C2,2′ and C4,2′. This choice is reinforced by noting that there are two curves in **3** that overlap at low temperatures and are most likely from nonterminal C3,2′ and C5,2′, in a similar sequence environment to the C-sugars in **4**. The current data cannot be used to further distinguish profiles from G2,2′, G4,2′, and C1,2′ in **3**; it is noteworthy that the present assignments consistently give the GC2′ small slopes.

In **1** there is a tightly interwoven set of four curves, two with small negative slopes and two with larger positve slopes; the former are tentatively identified with G3,2′ and G5,2′ and the latter with C4,2′ and C6,2′—these are all nonterminal residues having similarity in sequence environment to the GC2′ and CC2′ identified in **3** and **4**, as well as exhibiting similarly shaped δ *vs* T profiles. That leaves the lower group of three curves in **1** as originating from T1,2′, T7,2′, and A2,2′. Once C8,2′ in **2** has been identified, the nucleoside stoichiometry requires two GC2′, one CC2′, and two each of AC2′ and TC2′ to be assigned. In **1** it was clear that the T/A curves fall below the C/G profiles. Consistency requires that the four lower curves in **2** that coalesce at 80 °C be identified with TC2′ and AC2′ and the three higher curves (in the melted strands) be assigned to GC2′ and C7,2′ in accord with the stoichiometry. The C7,2′ profile must be the one with positive slope, and the G1,2′ and G2,2′ curves apparently have small negative slopes; these trends are all consistent among the four duplexes. The T1,2′ profile in **4** has a strong positive slope; this suggests that the curves labeled T3 and T5 in **2** (Figure 3) belong to the TC2′, which then identifies the negatively sloping profiles with A4,2′ and A6,2′. These observations lead to the final distinction among the C2′ group: that the curve labeled T1 of **1** (Figure 3) is similar to the curve labeled T1 of **4**, and may be so identified.

REFERENCES

Altona, C. (1987) *Nucleosides Nucleotides 6*, 157.

Ashcroft, J., LaPlante, S. R., Borer, P. N., & Cowburn, D. (1989) *J. Am. Chem. Soc. 111*, 363.

Ashcroft, J., Live, D. H., Patel, D. J., & Cowburn, D. (1991) *Biopolymers 31*, 45–55.

Bax, A., & Lerner, L. (1988) *J. Magn. Reson. 79*, 429.

Borer, P. N., Zanatta, N., Holak, T. A., Levy, G. C., van Boom, J., & Wang, A. H.-J. (1984) *J. Biomol. Struct. Dyn. 1*, 1373.

Borer, P. N., LaPlante, S. R.; Zanatta, N., & Levy, G. C. (1988) *Nucleic Acids Res. 16*, 2323.

Borer, P. N., LaPlante, S. R.; Kumar, A., Zanatta, N., Martin, A., Hakkinen, A., & Levy, G. C. (1994) *Biochemistry* (following paper in this issue).

Boudreau, E. A. (1992) Ph.D. Thesis, Syracuse University.

Calladine, C. R. (1982) *J. Mol. Biol. 161*, 343.

Cheng, D. M., Kan, L.-S., Frechet, D., Ts'o, P. O. P., Uesugi, S., Shindo, T., & Ikehara, M. (1984) *Biopolymers 23*, 1.

Cheong, C., Varani, G., & Tinoco, I., Jr. (1990) *Nature 346*, 680–682.

Dickerson, R. E. (1983) *J. Mol. Biol. 166*, 419.

Eimer, W., Williamson, J. R., Boxer, S. G., & Pecora, R. (1990) *Biochemistry 29*, 799–811.

Giessner-Prettre, C. (1985) *J. Biomol. Struct. Dyn. 3*, 145.

Gronenborn, A. M. & Clore, G. M. (1985) *Prog. NMR Spectrosc. 17*, 1.

Hyman, T. J., Boudreau, E. A., Martin, G. G., Jucker, B. M., Borer, P. N., & Levy, G. C. (1988) *J. Chem. Inf. Comput. Sci. 28*, 226.

Iwahashi, H., & Kyogoku (1976) *J. Am. Chem. Soc. 98*, 7761.

Kearns, D. R. (1987) in *Two-Dimensional NMR Spectroscopy* (Croasmun, W. R., & Carlson, R. M. K., Eds.) p 301, VCH Publishers, New York.

Lankhorst, P. P., Erkelens, C., Haasnoot, C. A. G., & Altona, C. (1983) *Nucleic Acids Res. 11*, 7215.

Lankhorst, P. P., van der Marel, G. A., van Boom, J. H., & Altona, C. (1985) *Nucleic Acids Res. 13*, 3317.

LaPlante, S. R. (1988) Ph.D. Thesis, Syracuse University.

LaPlante, S. R., Boudreau, E. A., Zanatta, N., Ashcroft, J., Cowburn, D., Levy, G. C., & Borer, P. N. (1988a) *Biochemistry 27*, 7902.

LaPlante, S. R., Ashcroft, J., Cowburn, D., Levy, G. C., & Borer, P. N. (1988b) *J. Biomol. Struct. Dyn. 5*, 1089.

Leupin, W., Wagner, G., Denny, W. A., & Wüthrich, K. (1987) *Nucleic Acids Res. 15*, 267.

Levy, G. C., & Nelson, G. L. (1972) *J. Am. Chem. Soc. 94*, 4897.

Levy, G. C., Lichter, R. L., & Nelson, G. (1980) *Carbon-13 Nuclear Magnetic Resonance Spectroscopy*, Wiley-Interscience, New York.

Levy, G. C., Hilliard, P. R., Jr., Levy, L. F., & Rill, R. L. (1981) *J. Biol. Chem. 256*, 9986.

Levy, G. C., Craik, D. J., Kumar, A., & London, R. E. (1983) *Biopolymers 22*, 2703–2726.
Newmark, R. A., & Cantor, C. R. (1968) *J. Am. Chem. Soc. 90*, 5010.
Orbons, L. H., Clore, G. M., Nilges, M., & Gronenborn, A. (1987) *J. Magn. Reson. 75*, 534.
Oschkinat, H., Clore, G. M., Nilges, M., & Gronenborn, A. (1987) *J. Magn. Reson. 75*, 534.
Patel, D. J., Shapiro, L., & Hare, D. (1986) *Biopolymers 25*, 693.
Petersen, S. B., Led, J. J. (1981) *J. Am. Chem. Soc. 103*, 5308.
Reid, B. R. (1987) *Q. Rev. Biophys. 20*, 1.
Rinkel, L. J., & Altona, C. (1987) *J. Biomol. Struct. Dyn. 4*, 621.
Rinkel, L. J., van der Marel, G. A., van Boom, J. H., & Altona, C. (1987a) *Eur. J. Biochem. 163*, 275.
Rinkel, L. J., van der Marel, G. A., van Boom, J. H., & Altona, C. (1987b) *Eur. J. Biochem. 166*, 87.
Saenger, W. (1984) *Principles of Nucleic Acid Structure*, Springer-Verlag, New York.
Schmitz, U., Zon, G., James, T. L. (1990) *Biochemistry 29*, 2537.
Schmitz, U., Kumar, A., & James, T. L. (1992) *J. Am. Chem. Soc. 114*, 10654.
Schmitz, U., Ulyanov, N. B., & James, T. L. (1993) *J. Biomol. Struct. Dyn. 10*, a171.
Siedman, K., & Maciel, G. (1977) *J. Am. Chem. Soc. 99*, 3254.
Sklenar, V., & Bax, A. (1987) *J. Am. Chem. Soc. 109*, 2221.
Stone, M., Winkle, S. A., & Borer, P. N. (1986) *J. Biomol. Struct. Dyn, 3*, 767.
Suzuki, E., Pattabiraman, N., Zon, G., & James, T. L. (1986) *Biochemistry 25*, 6854.
Varani, G., & Tinoco, I., Jr. (1991) *J. Am. Chem. Soc. 113*, 9349.
Wang, K. Y., Heffron, G. J., Bishop, K. D., Levy, G. C., Garbesi, A. M., Tondelli, L., Medley, J. H., & Borer, P. N. (1992) *Magn. Reson. Chem. 30*, 377–380.
Williamson, J. R., & Boxer, S. G. (1989) *Biochemistry 28*, 2819–2831.
Winstein, S., Carter, P., Anet, F. A. L., & Bourn, A. J. R. (1965) *J. Am. Chem. Soc. 87*, 5247.
Yanagi, K., Prive, G. G., & Dickerson, R. E. (1991) *J. Mol. Biol. 217*, 201–214.
Zanatta, N., Borer, P. N., & Levy, G. C. (1987) *Recent Advances in Organic NMR Spectroscopy* (Lambert, J. B., & Rittner, R., Eds.) pp 89–110, Norell Press, Landisville, PA.